Journal of Rock Mechanics and Geotechnical Engineering 8 (2016) 513–520

Contents lists available at ScienceDirect

Journal of Rock Mechanics and Geotechnical Engineering

journal homepage: www.rockgeotech.org

Full length article

Applications of FBG-based sensors to ground stability monitoring

An-Bin Huang, Chien-Chih Wang*, Jui-Ting Lee, Yen-Te Ho

Department of Civil Engineering, National Chiao Tung University, Hsin Chu, 30010, Taiwan, China

ARTICLE INFO

Article history:
Received 10 July 2015
Received in revised form
25 January 2016
Accepted 25 January 2016
Available online 26 May 2016

Keywords:
Monitoring
Ground stability
Subsidence

ABSTRACT

Over the past few decades, many optical fiber sensing techniques have been developed. Among these available sensing methods, optical fiber Bragg grating (FBG) is probably the most popular one. With its unique capabilities, FBG-based geotechnical sensors can be used as a sensor array for distributive (profile) measurements, deployed under water (submersible), for localized high resolution and/or differential measurements. The authors have developed a series of FBG-based transducers that include inclination, linear displacement and gauge/differential pore pressure sensors. Techniques that involve the field deployment of FBG inclination, extension and pore-pressure sensor arrays for automated slope stability and ground subsidence monitoring have been developed. The paper provides a background of FBG and the design concepts behind the FBG-based field monitoring sensors. Cases of field monitoring using the FBG sensor arrays are presented, and their practical implications are discussed.

1. Introduction

Most of the existing electrical sensor and cable systems are prone to adverse effects of electro-magnetic inference (EMI), short circuit, and lightning. The signal stability and system durability are especially important for field monitoring in geotechnical engineering where the sensors are often deployed in remote areas, permanently buried in the ground and under water. Maintenance or replacement of damaged field sensors can be costly. Adopting techniques from telecommunication systems, fiber optic sensors have features that are especially appealing for geotechnical field monitoring. A large number of fiber optic sensors can be installed in harsh environment and the system can be easily automated for data logging and transmission. Common drawbacks of the electrical sensors can be significantly and readily avoided when using the fiber optic sensors. Of the many available techniques, the authors have been concentrating on the use of fiber Bragg grating (FBG) as a core sensing element in their developments of a series of optic fiber sensored geotechnical field monitoring systems. This paper provides a brief background of FBG, presents the experiences in the application of various FBG sensored monitoring cases, and discusses the practical implication of FBG systems developed by the authors.

2. Methods

Optical fibers are made of silica, with a diameter about the same as that of a human hair, and can transmit light over long distances with very little loss of fidelity. Optical fibers comprise two essential components: a core and the surrounding annular cladding. The core of the optical fiber serves to guide light along the length of the optical fiber. The cladding has a slightly lower index of refraction than the core. Its primary function is to ensure total internal reflection within the core and that very little light is lost as it propagates along the core of the optical fiber. The typical combined diameter of core and cladding is 125 μm. The silica core/cladding is protected by an acrylic coating. The total outside diameter (OD) of an optical fiber with the acrylic coating is 250 μm. By adopting technologies from telecommunication, many fiber optic based sensing techniques have been developed. The optic FBG is one of the many available forms of optical fiber sensors. An FBG is created by a periodic variation of fiber core refractive index. The typical length of an FBG is 1–20 mm. When the FBG is illuminated by a wideband light source, a fraction of the light is reflected back upon interference by the FBG. The wavelength of the reflected light is linearly related to the longitudinal strains of the FBG (Rao, 1998), thus making FBG an ideal strain gage. The returned signal from every FBG carries a unique domain of wavelength, making it

* Corresponding author. Tel.: +886 935031129.
E-mail address: cc.wang.nctu@gmail.com (C.-C. Wang).

Peer review under responsibility of Institute of Rock and Soil Mechanics, Chinese Academy of Sciences.

http://dx.doi.org/10.1016/j.jrmge.2016.01.007

possible to have multiple FBG elements on the same fiber. The multiplexing among various sensors on a single fiber can be accomplished by wavelength division addressing, as conceptually described in Fig. 1. The FBG is partially distributive because only those parts of the optical fibers with FBG are used as strain sensors and these sensors can share the same optical fiber transmission line.

The FBG can be used directly as a strain gage, or, with the help of mechanical components, FBG can be configured as displacement, pressure and inclination transducers. All advantages of the FBG can be inherited in the FBG-based transducers for geotechnical engineering monitoring purposes. These advantages can include partially distributive, high resolution, good signal stability and immunity to EMI. The FBG-based sensors can be used as an individual sensor to reflect the physical quantity at a given location or connected into an array so that the profile of a given or multiple types of physical quantities can be monitored. The following sections describe some of the FBG-based transducers developed by the authors that are related to ground stability monitoring.

2.1. The FBG in-place inclinometer (FBG-IPI)

The FBG sensored pendulum type in-place inclinometer (FBG in-place inclinometer, FBG-IPI) was developed for the purpose of monitoring the variations of inclination in reference to gravity. As conceptually depicted in Fig. 2, a mass is linked to a hinge. A pair of FBGs is fixed to the sides of the mass. The FBG pair experiences elongation strains in opposite signs but equal amount when the mass is rotated away from verticality against the hinge. Thus, the FBG pair senses the amount of rotation and offsets the temperature effects. Fig. 3 shows the calibration result of the FBG-IPI.

2.2. The FBG pressure transducer

Fig. 4 shows a schematic view and photograph of an FBG pressure transducer. The FBG was used to sense the deflection of a metallic diaphragm inside the transducer due to changes in pressure against the atmosphere. A separate FBG was placed inside the transducer to monitor temperature fluctuations. The range of pressure transducer was controlled by the stiffness of the diaphragm. Fig. 5 shows the calibration result of the FBG pressure transducer.

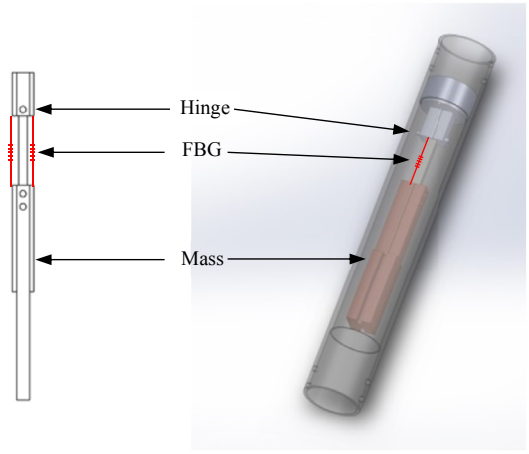

Fig. 2. Design of the FBG-IPI.

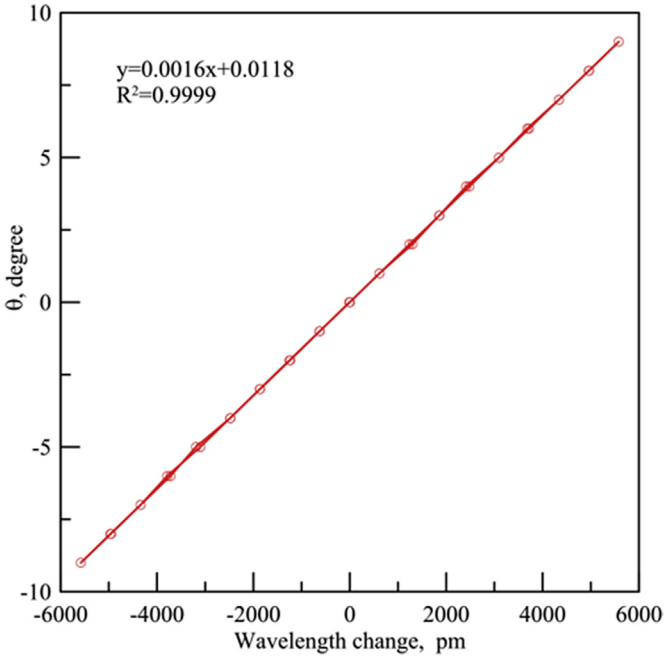

Fig. 3. Calibration of the FBG-IPI.

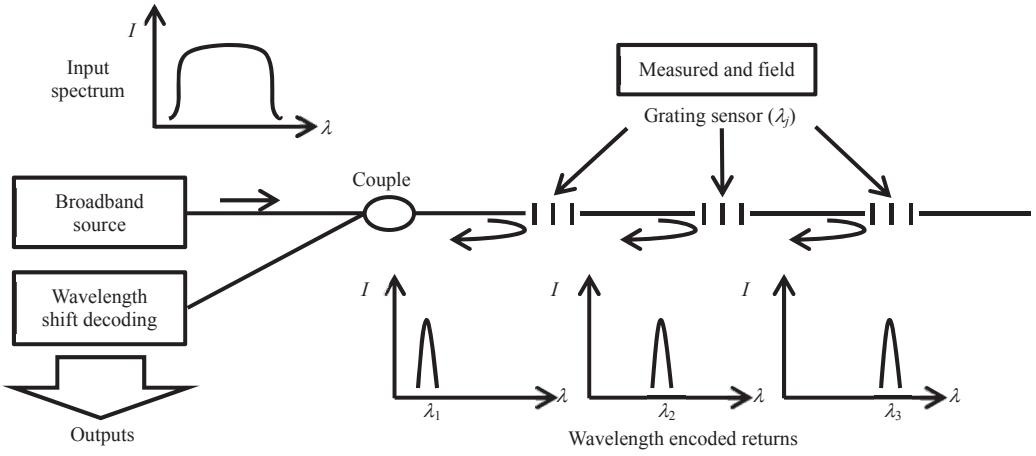

Fig. 1. Schematic diagram of FBG (adapted from Kersey, 1993), where I is the light intensity, and λ is the wavelength.

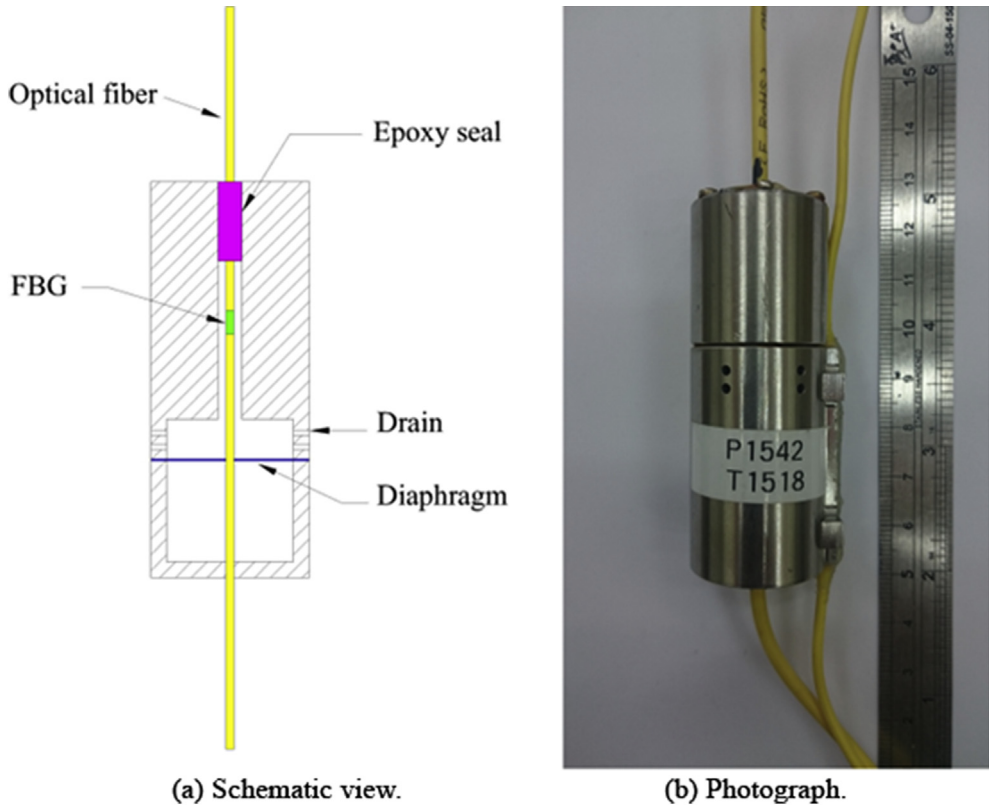

Fig. 4. The FBG pressure transducer.

2.3. The FBG extensometer

The FBG extensometer shown in Fig. 6 was developed to measure linear extension or compression. The linear movement induces relative motion between a roller and a wedge that in turn creates bending to a spring leaf. A pair of FBGs attached to the spring leaf was used to measure bending of the spring leaf, where the amount of linear displacement was deduced. Two pairs of spring leaves, separated by 180°, were used for extension and compression measurements. The device was designed to have a linear resolution of 8 μm, and a full range of 100 mm in compression and 50 mm in extension. Fig. 7 shows the calibration result of the FBG extensometer.

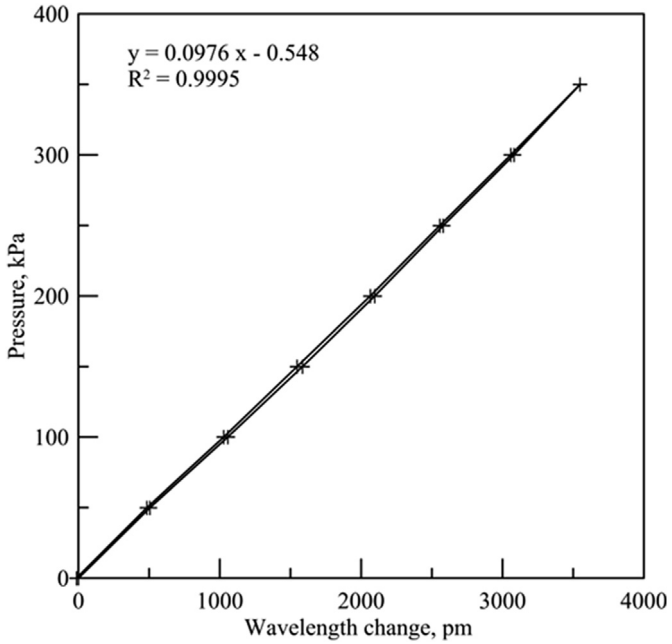

Fig. 5. Calibration of the FBG pressure transducer.

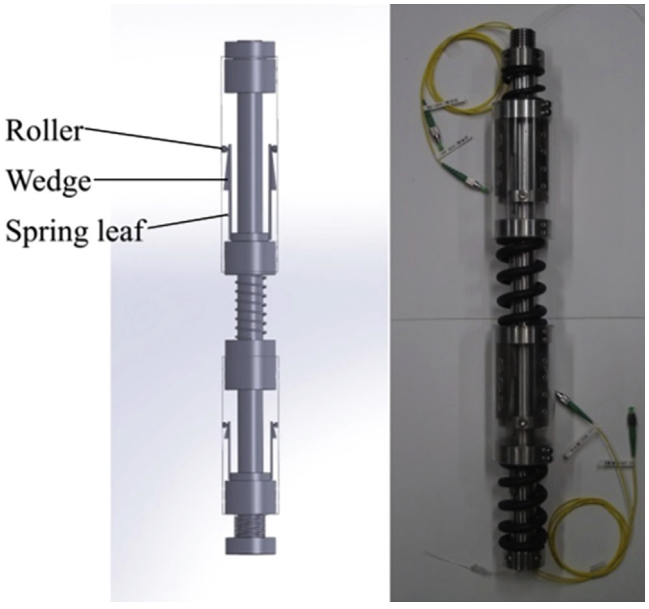

Fig. 6. The FBG extensometer.

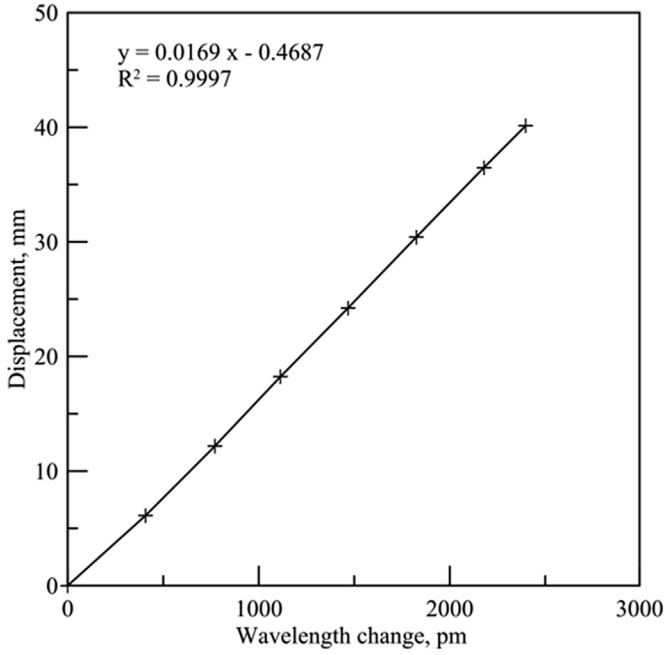

Fig. 7. Calibration of the FBG extensometer.

3. Results

3.1. Slope stability monitoring at Five Turn Point

A section of Highway 18, referred to as the Five Turn Point, has been selected as the most dangerous highway in Southern Taiwan, China. The slope area was approximately 1200 m by 1000 m where the ground surface elevation changed by as much as 400 m (see Fig. 8). At least eight sectors (designated as N1–N8 in Fig. 8) have been identified with either previous slope failure or signs of continuous movement. Fig. 9 depicts cross-sectional view of section *B-B* that has an average slope angle of 23°. The shear planes associated with earlier ground failures according to available investigations are also included in Fig. 9. Subsurface explorations revealed that the subject area was covered by 0–26 m of colluvial material underlain by interlayered fractured sandstone and shale extended from below the colluvial to over 200 m (deepest borehole available) below the ground surface. Because of the wide range in sizes of the fractured rock pieces, it was not possible to obtain good

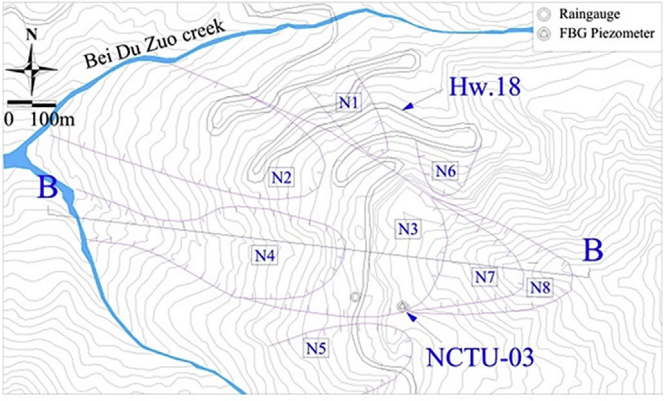

Fig. 8. Topographic map of the Five Turn Point (after Land Engineering Consultants Co., Ltd., 2007).

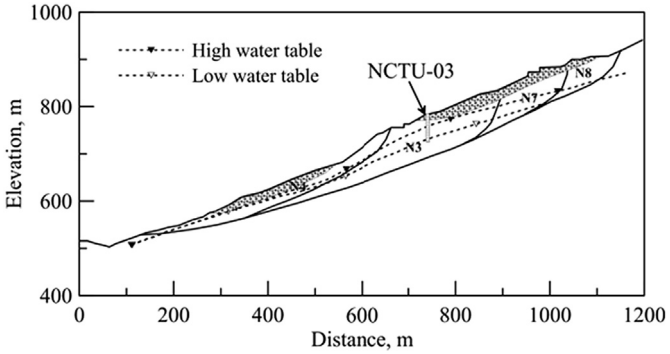

Fig. 9. Section *B-B* of the Five Turn Point (after Land Engineering Consultants Co., Ltd., 2007).

quality samples for laboratory shearing tests and to provide representative strength parameters. The groundwater could rise from its low level by more than 20 m as a result of heavy rainfalls according to available open-end piezometer data shown in Fig. 9. The sudden and significant change in groundwater table is believed to be a major cause for the earlier slope failures in this area.

A 60 m deep borehole marked as NCTU-03 in Figs. 8 and 9 was used to install the FBG piezometer array. The FBG pressure transducer, used as a piezometer, was fitted inside a PVC pipe with the inner diameter of 28 mm and outer diameter of 32 mm. Small drainage holes were drilled in the PVC pipe and wrapped with non-woven geotextile in areas surrounding the piezometer to allow passage of water. The piezometer was epoxied and sealed at both ends in the PVC pipe to prevent seepage between piezometers from within the PVC pipe. The PVC pipe serves as a spacer and houses for the piezometers and optical fiber. Final assembly was made as the PVC pipe was lowered into the borehole. A comparison between an array of FBG piezometers installed in a single borehole to the case of individual standpipe is depicted in Fig. 10. An array of FBG-IPI was also installed close to NCTU-03, at depths from 30 m to 60 m. All sensors were connected to an on-site computer using optical fiber cables for optical signal interrogation and data logging/transmission. A funnel and a tremie pipe were used to inert sand drain around the piezometers and bentonite pallets to seal the borehole between the piezometers. Fig. 11a shows the insertion of sand drain material via the funnel and the tremie pipe. A photograph of FBG piezometers packaged inside the PVC pipes and ready for installation is shown in Fig. 11b. More details on the field installation of FBG piezometer array can be found in Huang et al. (2012). Field installation was completed in September 2007.

The Five Turn Point slope has endured three major typhoons (i.e. Sinlaku of 2008, Morakot of 2009, and Fanapi of 2010) since September 2008, and remained stable till December 2015. Of the three typhoon events, Morakot was the most damaging. A histogram of daily precipitations during typhoon Morakot at Five Turn Point is shown in Fig. 12. Fig. 13 shows a set of representative pressure head (h_p) profiles based on the FBG piezometer readings recorded from the beginning of typhoon Morakot to the time when h_p reached the maximum value.

The pore water pressure readings enabled the concept of field stress path (Anderson and Sitar, 1995; Cascini et al., 2010) to be used in evaluating the stability of a slope. The initial state of stress at each of the pore water pressure measurement locations was computed using the commercial software SIGMA/W (GEO-SLOPE International Ltd, 2007). The computation was based on the cross-section shown in Fig. 9. The ground material was assumed to be linear elastic with the Young's modulus $E = 3310$ MPa, Poisson's ratio $\mu = 0.35$, and the total unit weight $\gamma = 2\gamma_w$, where γ_w is the

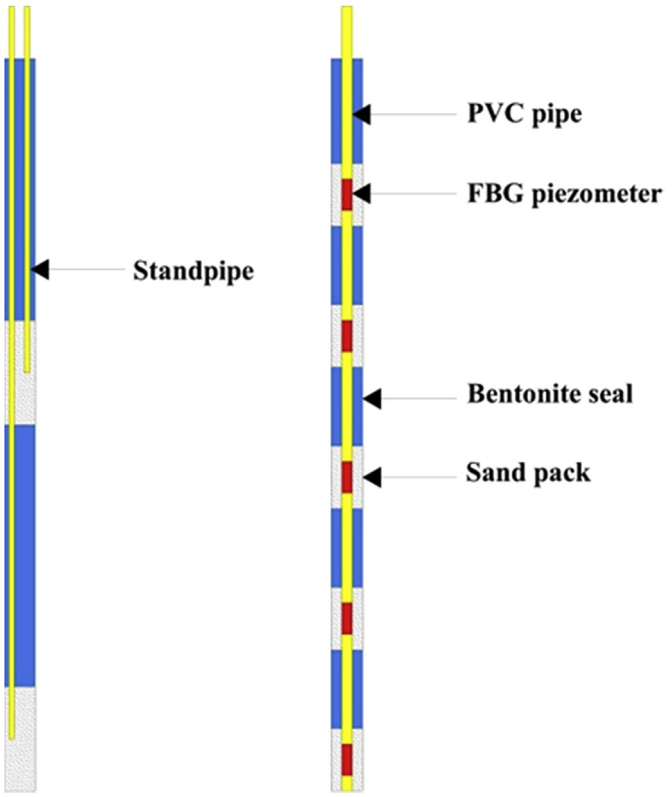

Fig. 10. Comparison between the individual standpipe and piezometer array installations.

unit weight of water. For simplification, the single γ value used in the computation reflects a saturated state even when the material could be unsaturated. The potential error from this simplification is insignificant in comparison with the stress level and the effects of pore water pressure variations (Anderson and Sitar, 1995). Considering a plane strain condition, p' and q were calculated as

$$p' = (\sigma'_1 + \sigma'_2 + \sigma'_3)/3 \tag{1}$$

$$q = \frac{1}{\sqrt{2}}\sqrt{(\sigma'_1 - \sigma'_3)^2 + (\sigma'_1 - \sigma'_2)^2 + (\sigma'_2 - \sigma'_3)^2} \tag{2}$$

where σ'_1, σ'_2 and σ'_3 are the major, intermediate and minor principal stresses, respectively.

As the measured pore water pressure increases, q at a given measurement point remains constant while p' decreases and the corresponding stress point (p', q) moves laterally towards a failure envelope as shown in Fig. 13. The (p', q) points depicted in Fig. 13 correspond to the respective nine FBG piezometer locations installed in the field. The lower left (p', q) points represent the state of field stress at shallower depths. The results also show a potential failure envelope that corresponds to a ϕ' value of 40°. Although not necessary for the Five Turn Point case, variations in slope angle and ground layers can be readily incorporated in the analysis under the framework of field stress path. It should be noted that the outcome of the linear elastic stress analysis was not sensitive to the selection of Young's modulus. However, the selection of Poisson's ratio could have significant effects on the initial p' and q values.

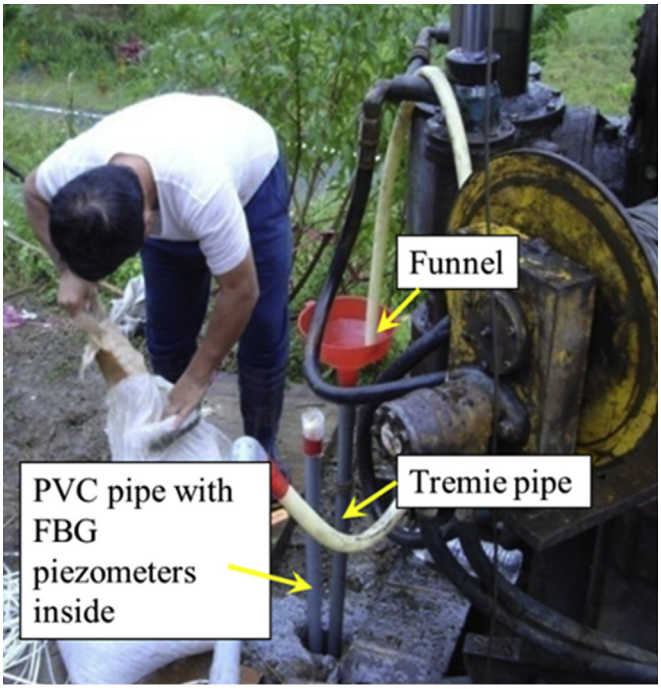

(a) Insertion of sand drain material via a funnel and tremie pipe.

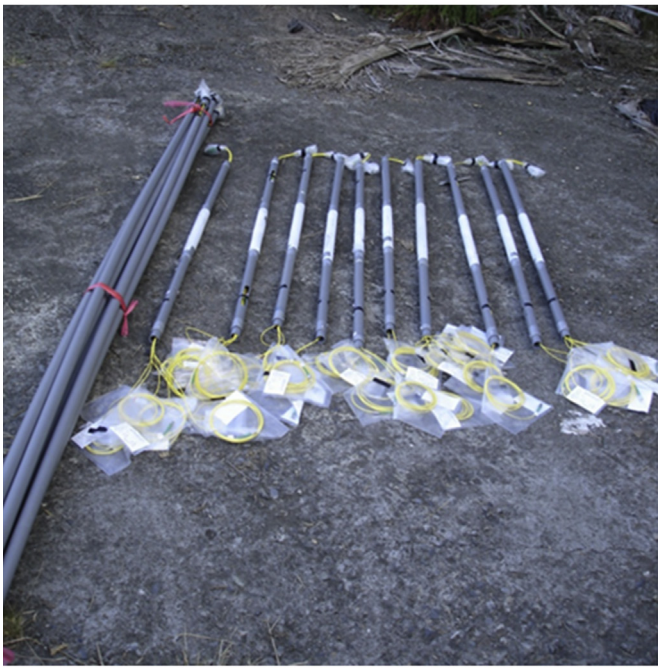

(b) The packaged FBG sensor array.

Fig. 11. Field installation of the FBG piezometer array.

3.2. Ground subsidence monitoring at Guan-Fu elementary school

Guan-Fu elementary school is located in Yun Lin County of Central Western Taiwan, China as shown in Fig. 14, the heart of an area where the ground subsidence was the most significant in the Island. From 1992 to 2010, the accumulated subsidence was as much as 900 mm. The alluvial soil deposit in this region is expected to be more than 1000 m thick. Excessive groundwater pumping was believed to be the main cause of such ground subsidence. In

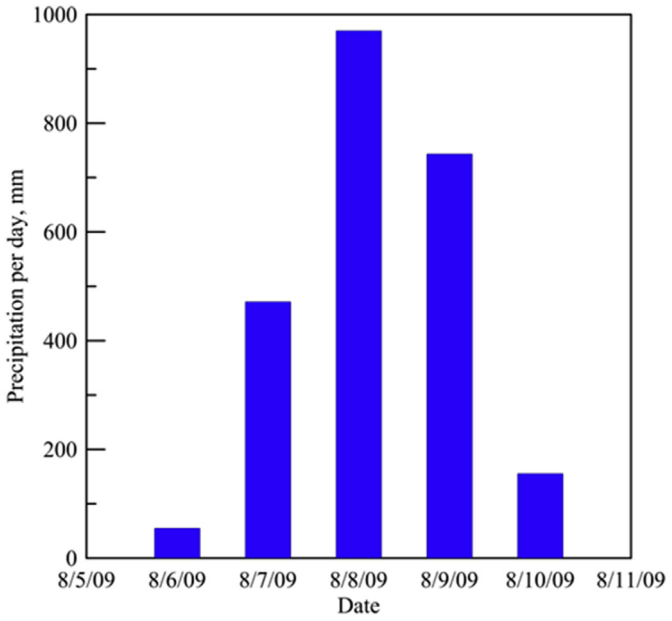

Fig. 12. Rainfall record during typhoon Morakot (Huang et al., 2012).

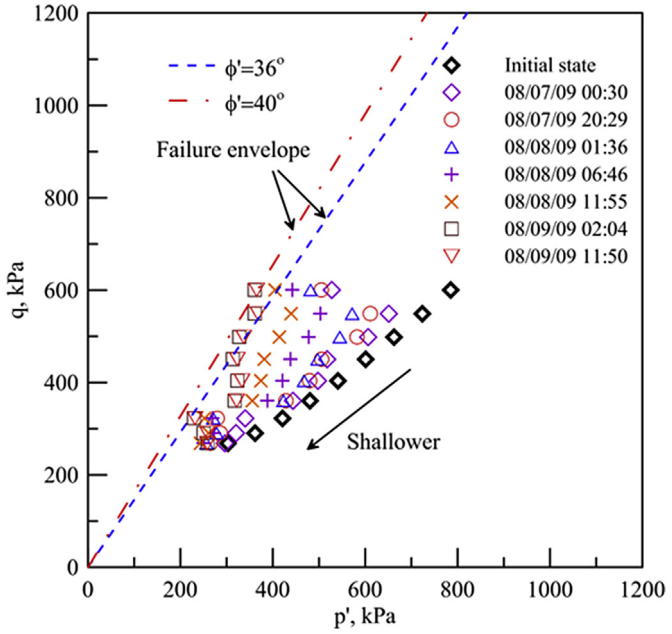

Fig. 13. Evolution of field stress paths during typhoon Morakot (Huang et al., 2012), where ϕ' is the effective friction angle.

order to ascertain the mechanisms of ground subsidence, the traditional magnetic rings and SONDEX sensor probe have been used to measure the ground settlement profile manually. Boreholes extending to a maximum depth of 300 m have been used for this purpose. Open-end piezometers, with a maximum number of 3, have been installed at selected depths to provide reference pore water pressure values. The metal tape and SONDEX measurement system had a resolution of 1 mm and repeatability of ±4 mm. Because of the deficiency in measurement resolution and mismatch between settlement and pore water pressure measurement depth frequencies, rigorous interpretation of the observed data was difficult. In any case, the government had shut down

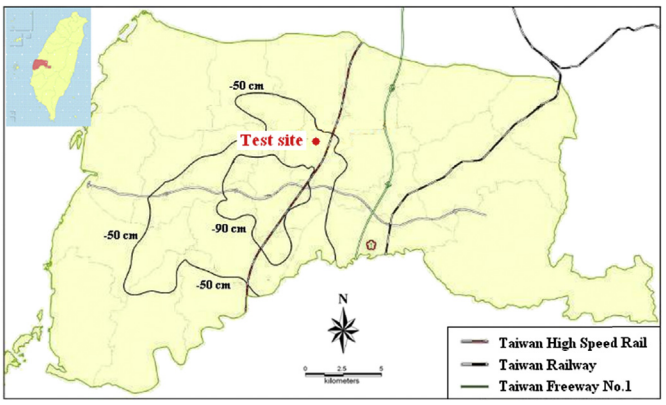

Fig. 14. The test site in Yun Lin County of Central Western Taiwan, China and contours of ground subsidence from 1992 to 2010 (after Water Resources Agency, Taiwan, 2010).

pumps installed below the depth of 50 m in 2010. These deep wells had large capacities and had been used to provide water for the local industries. SONDEX measurements and surface elevation survey taken since 2012 showed that the ground surface settlement in the project area has been reduced to less than 3 mm per year. Shallow pumps installed in depth range from 30 m to 50 m, mainly used by the local farmers for irrigation purposes, remained operational.

As a trial project, the authors installed an FBG ground subsidence monitoring array at the depth of 100 m at the Guan-Fu elementary school test site. In this array, the FBG extensometers shown in Fig. 6 were connected to a plastic pipe with the length of 10 m, outer diameter of 100 mm, and inner diameter of 80 mm, as schematically shown in Fig. 15a. The pipe was equipped with friction rings, spaced at 2 m to increase grip between the plastic pipe and the surrounding soil. An FBG piezometer was installed at the middle of each plastic pipe. Field installation of the FBG ground subsidence monitoring array (see Fig. 15b) was completed on April 26, 2012. The settlement readings taken within 4 months after the installation were disarrayed which was believed to have been caused by the rearrangement of the soil disturbed by the field installation. Fig. 16 depicts the pore water pressure and ground settlement profiles according to the monthly readings from September 30, 2012 to December 2013. Fig. 16 shows that the pore water pressure increased consistently with time at all depths. This increase in pore water pressure is apparently induced due to the shut-down of deep and powerful pumps in the region. It should be noted that all subsidence readings were in reference to the bottom of the sensor array (100 m below the ground surface). Subsidence measurements can be divided into three segments: 0–30 m, 30–50 m and 50–100 m. The soil in 0–30 m and 50–100 m showed heaving during the monitoring period. The heaving was reasonable as the pore pressure increased in the same period. However, the soil in 30–50 m depth range was still settling even though the general trend indicated that the pore pressure was increasing. The reason for such behavior was not immediately clear.

Although excessive groundwater pumping was believed to be the main reason for earlier ground subsidence in the region, the soil deposit was mostly granular with various amounts of fines (particles passing #200 sieve) as indicated in Fig. 16. According to Fig. 16, the groundwater table should be located at approximately 6 m below the ground surface, if the groundwater table was taken as the level where the pore water pressure was zero. According to the information provided by local farmers, this groundwater table remained stable in the past few decades. It was thus not reasonable to attribute the earlier ground subsidence to conventional thinking

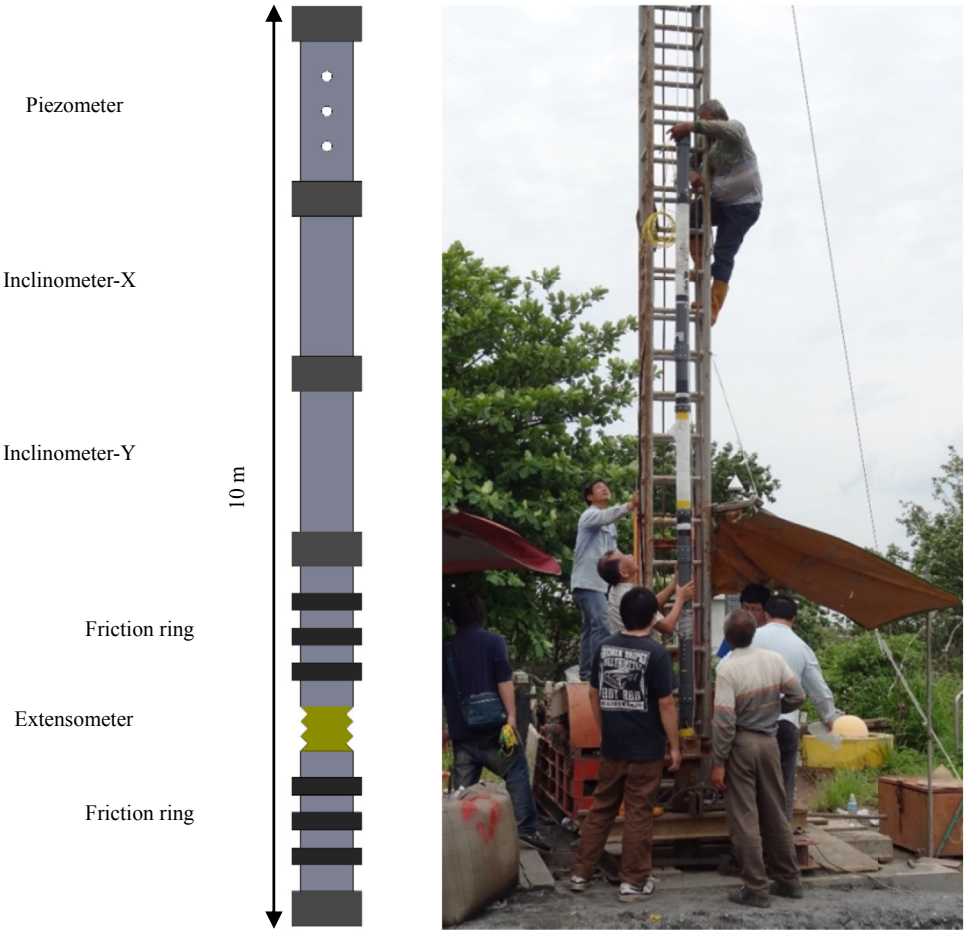

(a) Schematic view of the sensor array. (b) Field installation of the subsidence sensor array.

Fig. 15. Field installation of the FBG ground subsidence monitoring array.

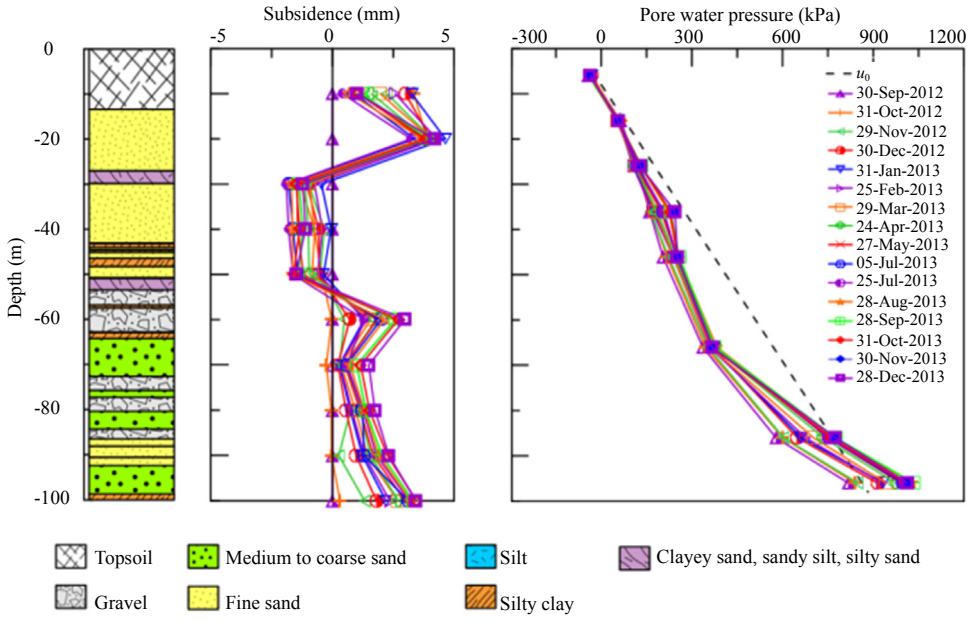

Fig. 16. Pore water pressure and ground settlement profiles with boring log.

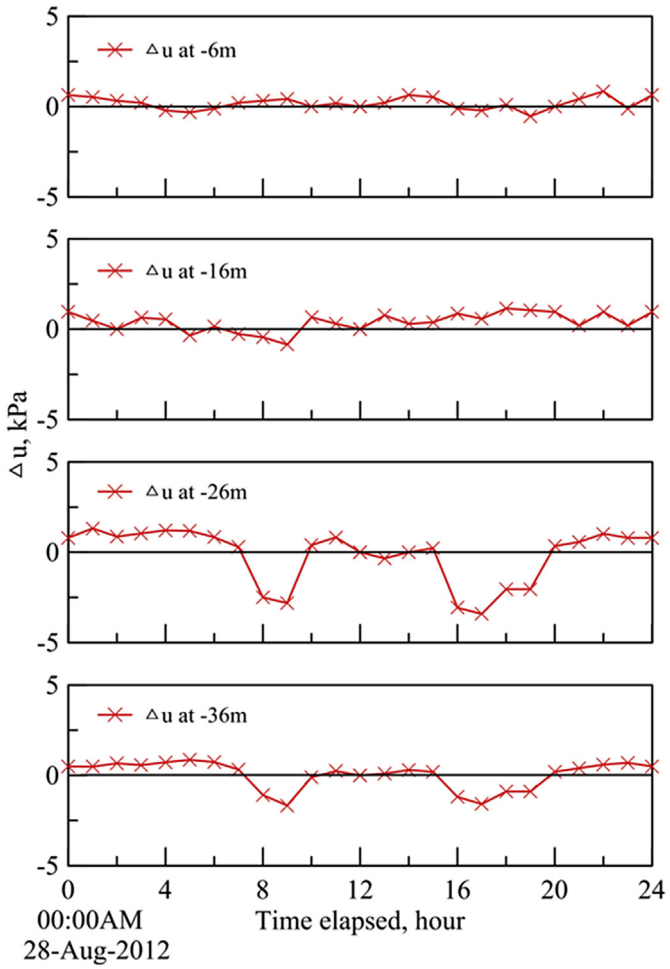

Fig. 17. 24 h continuously readings of pore water pressure.

of consolidation of compressible cohesive soil layers (such as normally consolidated clays) due to lowering of groundwater table. The ground subsidence was thus more likely to have been caused by the compression of the granular material due to lowering of pore water pressure and hence the increase of effective overburden stress at its depth. For these premises to be valid, the granular material must have very high compressibility and/or the pore water pressure lowers significantly. The granular soil in this region was mostly silica in nature and was not known to be excessively compressible. The previous open-end piezometer readings did not indicate excessive lowering of groundwater table. Because of these reasons, it was difficult to conclude why and how the earlier ground subsidence occurred, at least based on our current readings.

Fig. 17 shows a typical set of 24 h continuous readings of pore water pressure taken at the site. The results showed that the pore water pressure fluctuated repeatedly in the morning and evening at depths between 20 m and 40 m. It was suspected that this fluctuation of pore water pressure was related to the on-and-off type of groundwater pumping from wells within comparable depth range nearby. The authors suspected that this repeated on-and-off pumping induced repeated loading and unloading to the nearby granular soils similar to the case of traffic load on pavement. The repeated loading/unloading, albeit small in magnitude, can cause accumulation of permanent subsidence (Tao et al., 2010), a phenomenon often referred to as “shakedown”. Triaxial tests on the granular soil samples taken from the site are underway. In these triaxial tests, the soil specimen was subjected to repeated fluctuation of pore water pressure while monitoring its strain accumulation. Field pressure meter tests are also being carried out at various depths with repeated loading and unloading. The tests have not been completed and their interpretation is beyond the scope of this paper. However, this repeated pore pressure fluctuation in the 30–50 m depth range was believed to be the cause for the small amount of settlement, even though the pore water pressure was increasing on a long term basis. The same mechanism may also be able to explain the much more significant ground subsidence due to the on-off deep well water pumping at much high capacities.

4. Conclusions

The experience shows that with the help of partially distributive sensors, field pore water pressure profile monitoring can be practically implemented. Taking advantage of the pore water pressure profile values, a stress based warning of a potential slope failure can be implemented. The stress based warning system considers the proximity between the current state of stress and failure envelope of the field material. We no longer rely solely on lateral displacement measurement as a means to project slope failure, as it has typically been done before.

The integrated simultaneous pore water pressure and ground subsidence profile measurements provide real-time data that can readily be used to analyze the potential mechanism or cause for ground subsidence.

Conflict of interest

The authors wish to confirm that there are no known conflicts of interest associated with this publication and there has been no significant financial support for this work that could have influenced its outcome.

References

Anderson SA, Sitar N. Analysis of rainfall-induced debris flows. Journal of Geotechnical Engineering 1995;121(7):544–52.
Cascini L, Cuomo S, Pastor M, Sorbino G. Modeling of rainfall-induced shallow landslides of the flow-type. Journal of Geotechnical and Geoenvironmental Engineering 2010;136(1):85–98.
GEO-SLOPE International Ltd. SIGMA/W for stress-deformation. Version 7.17. User’s guide. Calgary, Canada: GEO-SLOPE International Ltd.; 2007.
Huang AB, Lee JT, Ho YT, Chiu YF, Cheng SY. Stability monitoring of rainfall induced deep landslides through pore pressure profile measurements. Soils and Foundations 2012;52(4):737–47.
Kersey AD. Multiplexed fiber optic sensors. Proceedings of SPIE (Vol. 1797): Distributed and Multiplexed Fiber Optic Sensors II 1993. http://dx.doi.org/10.1117/12. 141286.
Land Engineering Consultants Co., Ltd. Highway 28.9K–31.5K (Five Turn Point) landslide investigation, remediation planning and safety evaluation. 3rd overall report. Department of Highway Maintenance; 2007 (in Chinese).
Rao YJ. Fiber Bragg grating sensors: principles and applications. In: Grattan KTV, Meggitt BT, editors. Optic fiber sensor technology, vol. 2. London: Chapman and Hall; 1998. p. 355–79.
Tao M, Mohammad L, Nazzal M, Zhang Z, Wu Z. Application of shakedown theory in characterizing traditional and recycled pavement base materials. Journal of Transportation Engineering 2010;136(3):214–22.
Water Resources Agency, Taiwan. 2010 report on ground subsidence monitoring, investigation and analysis for Chanhwa, Yunlin, Chiayi and Tainan areas. Hsinchu, Taiwan. 2010 (in Chinese).